University of California
Ernest O. Lawrence Radiation Laboratory

PION-PROTON CHARGE-EXCHANGE SCATTERING FROM 500 TO 1300 MeV

TWO-WEEK LOAN COPY

This is a Library Circulating Copy which may be borrowed for two weeks. For a personal retention copy, call Tech. Info. Division, Ext. 5545

Berkeley, California

DISCLAIMER

This document was prepared as an account of work sponsored by the United States Government. While this document is believed to contain correct information, neither the United States Government nor any agency thereof, nor the Regents of the University of California, nor any of their employees, makes any warranty, express or implied, or assumes any legal responsibility for the accuracy, completeness, or usefulness of any information, apparatus, product, or process disclosed, or represents that its use would not infringe privately owned rights. Reference herein to any specific commercial product, process, or service by its trade name, trademark, manufacturer, or otherwise, does not necessarily constitute or imply its endorsement, recommendation, or favoring by the United States Government or any agency thereof, or the Regents of the University of California. The views and opinions of authors expressed herein do not necessarily state or reflect those of the United States Government or any agency thereof or the Regents of the University of California.

Submitted to Physical Review

UCRL-17209 Rev.

UNIVERSITY OF CALIFORNIA

Lawrence Radiation Laboratory
Berkeley, California

AEC Contract No. W-7405-eng-48

PION-PROTON CHARGE-EXCHANGE SCATTERING FROM 500 TO 1300 MeV

Charles B. Chiu, Richard D. Eandi, A. Carl Helmholz,
Robert W. Kenney, Burton J. Moyer, John A. Poirier,
W. Bruce Richards, Robert J. Cence, Vincent Z. Peterson,
Narender K. Sehgal, and Victor J. Stenger

January 1967

Pion-Proton Charge-Exchange Scattering From 500 to 1300 MeV*

Charles B. Chiu, Richard D. Eandi, A. Carl Helmholz, Robert W. Kenney, Burton J. Moyer, John A. Poirier,† and W. Bruce Richards‡

Lawrence Radiation Laboratory, University of California, Berkeley, California

and

Robert J. Cence, Vincent Z. Peterson, Narender K. Sehgal, and Victor J. Stenger

University of Hawaii, Honolulu, Hawaii

ABSTRACT

Differential cross sections for the reaction $\pi^- p \rightarrow \pi^0 n$ were measured at nine incident-pion kinetic energies in the interval from 500 to 1300 MeV. The negative pion beam from the Bevatron was focused on a liquid hydrogen target completely surrounded by a cubic array of six steel-plate spark chambers. The spark chambers were triggered on events with neutral final states. Charge-exchange events were identified from the one-shower and two-shower events in the spark-chamber pictures. By the Monte Carlo technique, the π^0 distributions were calculated from the bisector distributions of the two-shower π^0 events together with the observed gamma-ray distributions of the one-shower π^0 events. These π^0 distributions were fitted with both Legendre polynomial expansions and power-series expansions by the method of least squares. The extrapolated forward differential cross sections are in good agreement with the dispersion calculations. The Legendre coefficients for the differential

cross sections in isospin state T = 1/2 were obtained by combining our results with available data on $\pi^{\pm}p$ elastic scattering. In the light of existing phase-shift solutions, the behavior of these coefficients is discussed. The D_5F_5 interference term that peaks near 900 MeV is verified to be in isospin state T = 1/2 only.

We report here also the total neutral cross sections and the cross sections for the production of neutral multipion final states, $2\pi^{o}n$ and $3\pi^{o}n$. The 4π solid angle and the calibrated energy response of the spark chambers contribute to the accuracy of the results.

I. INTRODUCTION

In the past several years much work has been done to further our knowledge of the apparent resonances at 600 and 900 MeV in π-N scattering. Systematic studies have been made of the elastic differential cross sections[1-4] and the polarization of the recoil proton[4, 5] near these two resonances. A knowledge of the charge-exchange cross section is also necessary in order to help resolve the ambiguities inherent in phase-shift analyses. More explicitly, the charge-exchange differential cross section must be known along with elastic scattering in order to deduce the differential cross section for scattering in the isospin state T = 1/2.

Some measurements have already been reported. These include forward charge-exchange cross sections measured with spark chambers between 0.8 and 1.9 GeV[6] and the angular distribution in charge-exchange scattering near 900 MeV measured in bubble chambers.[7, 8] The angular distributions in the reaction $\pi^+ n \rightarrow \pi^0 p$ were also measured in a deuterium bubble chamber between 600 and 900 MeV.[9] Simultaneous with the experiment to be reported here, the angular distributions in $\pi^- p \rightarrow \pi^0 n$ scattering were measured at 10 energies between 545 and 1151 MeV, using an array of spark chambers.[10] We report here a similar experiment in which we measured the angular distributions in charge-exchange scattering at nine energies between 500 and 1311 MeV.[11]

The spark-chamber array used in this experiment completely surrounded the liquid-hydrogen (LH_2) target. This is in contrast to the experiment of Ref. 10 in which the spark-chamber array subtended about 2/3 of 4π solid angle. This is an important difference between the two experiments. We shall see that while the results of the two experiments are in general agreement, there are significant differences in detail.

Cross sections and the angular distributions for η production, $\pi^- p \rightarrow \eta^o n$ were also obtained from this same run and film. The η results have been presented in a separate paper.[12]

II. EXPERIMENTAL PROCEDURE AND APPARATUS[13]

A. Procedure

The layout of the experiment is shown in Fig. 1. Negative pions produced from a target inside the Bevatron were deflected out, momentum-analyzed, and focused through a series of magnets, then delivered first to the target of another experiment, and finally refocused at our LH_2 target. The incident pion flux was defined by a triple coincidence of three counters, M_1, M_2, and M_3, together with a ring anticounter A_0, to define the area of the beam. The LH_2 target was placed at the center of a cubic spark-chamber assembly consisting of six iron-plate chambers, each about six radiation lengths thick. Inside the assembly, the downstream half of the target was surrounded by a scintillation anticounter unit A_{1-9} subtending a solid angle of slightly more than 2π about the downstream side of the target. The spark-chamber assembly was triggered whenever the beam counters indicated a pion had entered the target and A_{1-9} indicated that no charged particle had emerged in the forward hemisphere. About 50% of the spark-chamber photographs showed only gamma-ray showers from $\pi^- p \rightarrow \pi^0 n$ ($\pi^0 \rightarrow 2\gamma$). From the observed spatial distributions of these gamma rays, the angular distributions of the π^0's were deduced.

B. Apparatus

1. Beam

The negative pion beam was momentum-analyzed and focused by three triplet quadrupole magnets and two bending magnets. The pion mean kinetic energies were determined by both wire-orbit measurements and the fitting of the $\pi^0 \rightarrow 2\gamma$ and $\eta \rightarrow 2\gamma$ opening-angle distributions. The

various values agreed within errors. Above the η threshold, the opening-angle values were adopted as being most precise. The momentum spread ($\Delta p/p$) was 5% (full width at half height). Typical pion flux under running conditions was 10^4 per Bevatron pulse. The electron and muon contamination at each pion energy was determined by means of a gas Cerenkov counter filled with SF_6. The anticounters surrounding the target eliminated electron and muon events. The sum of the electron and muon contaminations ranged from 15 to 40%. These corrections were applied to the beam monitor counts to obtain the corrected pion flux.

2. Counters and Electronics

Counters M_1, M_2, M_3, and A_0 were placed along the beam path to define the beam as shown in Fig. 1. Counters M_1 and M_2, at the two ends of quadrupole magnet Q_3, detected all the pions passing through the quadrupole. Anticounter A_0, with a 4-in.-diam hole aligned with the 4-in. hole of the entrance spark chamber, was used in anticoincidence with M_1, M_2, and M_3 to prevent the system from accepting events in which pions had interacted in the steel portion of the entrance chamber and scattered into counter M_3. Counter M_3, the last beam-defining counter, was a circular scintillator 2 in. in diameter and 1/16-in. thick and was placed inside the spark-chamber cube close to the window of the vacuum jacket (see Sec. B.3). A block diagram of the electronics is shown in Fig. 2. A coincidence between signals from counters M_1, M_2, and M_3, together with a null signal from anticounter A_0, defined an incident pion. These were counted by the scaler labelled "Mon. scaler" in Fig. 2.

Anticounters A_{1-9} covered the entire hemisphere downstream from the target. Although the counter array subtended a solid angle

only slightly greater than 2π steradian, charged final states, with all the charged particles missing the unit, were estimated to be small. It was kinematically impossible for both of the charged particles in two-body final states to miss the anticounters. Thus, contamination of the charged final states had to come from three-or-more-body final states. The most abundant three-body final state in the energy region of this experiment was $\pi^+\pi^-n$. Previous data indicated that those events with both $\pi^+\pi^-$ going into the backward hemisphere could contribute no more than 2% to our spark-chamber events.[14] In most cases these events could be recognized on the film and were excluded from the data. A null signal from anticounters A_{1-9}, together with an incident-pion signal, defined a neutral event. These were counted by the scaler labelled "Neut. scaler" in Fig. 2.

The coincidence circuit, W_3 in Fig. 2, triggered the spark chamber and turned on the camera control unit. The input signals to W_3 consisted of the neutral signal from the output of W_2 and two anticoincidence gate signals with long widths. One gate signal with a width of ≈ 2.5 μsec (approximately equal to the sensitive time of the spark chambers) was induced by the signal of counter M_2. Since M_2 covered the entire transverse cross section of the beam envelope, no pictures were taken for those neutral events where other beam particles had passed through the system in the previous 2.5 μsec. This greatly reduced the number of pictures with multiple incident-beam tracks. The other long input signal for W_3 was about 90 msec wide. This signal, generated by the output of W_3, prevented the spark chamber from firing while the film was being advanced.

3. Target

The inset on Fig. 3 shows the LH_2 target. The average thickness of the target over the area defined by counter M_3 was 3.93 ± 0.01 in. Because of bubbling, the density of liquid hydrogen was estimated to be $5 \pm 3\%$ less than the handbook value. The entire target was enclosed in a 2-ft.-diam Al vacuum jacket. The windows of the vacuum jacket were far enough from the LH_2 flask that "window events" could be identified by extrapolating the shower direction back to the target.

4. Spark Chambers and Optical System

The spark-chamber array is shown in Fig. 3. It consisted of six 5-ft.-square spark chambers. Two spark chambers each had an extra "dog leg" to complete the cubic array. The chambers were filled with a mixture of 90% Ne and 10% He.

A spark-chamber unit consisted of one 1/32-in. Al cover plate, four 1/16 in. Al plates, and thirty-five 1/8-in. Fe plates. There were 38 active gaps for detecting particles. To allow the incoming pions to pass through, one chamber had 4-in. concentric holes cut in the plates. The holes were covered with thin Al foils. The gap width was 5/16-in. and the plate voltage was about -9 kV.

Every spark chamber had two mutually perpendicular optical windows, each covered by a plano-convex Lucite field lens. Thirty-six plane mirrors brought all 12 views of the chambers to a single camera which photographed them on a double frame of 35-mm film.

III. DATA ANALYSIS

A. Uncorrected π^0 Distributions

All photographs of events showing one incoming pion and one or more outgoing tracks were scanned and recorded. Events with 1, 2, or 3 outgoing tracks were measured on digitized measuring projectors. Half of the events were measured in Berkeley and half in Hawaii. The two groups differed somewhat in their minimum criterion for a track. The Berkeley group demanded that a track have at least three sparks on a straight line. The Hawaii group demanded three sparks in consecutive gaps on a straight line.

Usually the $\pi^0 n$ final state gave a 2-track event resulting from $\pi^0 \rightarrow 2\gamma$ giving 2 showers in the steel. About a third of the time, however, one gamma ray had small enough energy so that no visible track was produced. (Zero-shower events are negligible at these energies.) For purposes of analysis it proved to be adequate, for these 1-track events, to assume that the π^0 direction was coincident with the visible-shower direction.

In general, the opening angle, ϕ, between the two photons in the barycentric system follows a probability distribution given by

$$dn/d\phi = \frac{\cos(\phi/2)}{2\,\beta\gamma^2 \sin^2(\phi/2)\left[\beta^2 - \cos^2(\phi/2)\right]^{1/2}}, \qquad (1)$$

where βc is the π^0 velocity and $\gamma^{-1} = (1 - \beta^2)^{1/2}$, all in the barycentric system. The distribution $dn/d\phi$ diverges at an angle for which $\cos(\phi_{min}/2) = \beta$. Instrumental resolution broadens this distribution somewhat, and reduces the peak to a finite value, as shown in Fig. 4.

The π^0 velocity vector lies in the plane of the two photons and within the included angular range. For given photon directions, the π^0 is least energetic when its momentum lies along the bisector of the opening angle.

A fraction of the final neutrons interacted in one of the steel plates producing a charged secondary and thus gave a 3-track event. This fraction ranged from 0.01 at the lowest energy to 0.11 at the highest energy. These events could be identified kinematically, since only two neutron directions are possible for given gamma-ray directions.

To be accepted for analysis the events had to satisfy certain criteria:

(1) The shower directions had to point back to the region of the LH_2 target. The size of this region depended on the length of the shower and was larger than the target to account for measurement errors.

(2) The showers had to begin in the Fe plates of the spark chambers with an allowance made for measurement errors.

(3) In 2-shower events the opening angle of the 2 showers in the barycentric system had to lie between (ϕ_{min} - 5 deg) and ϕ_{max}, where ϕ_{min} is the minimum angle allowed by kinematics, and ϕ_{max} is an angle such that ϕ_{max} exceeds ϕ for 75% of the events. The opening-angle distribution obtained at T_π^{lab} = 655 MeV is shown in Fig. 4. For our energies we have 21 deg $\leq \phi_{min} \leq$ 37 deg and 32 deg $\leq \phi_{max} \leq$ 54 deg.

In the reconstruction of the events in space, we assumed that all events originated at the point where the incoming pion crossed the mid-plane of the LH_2 target. The maximum resulting c.m. angular error was $\Delta(\cos\theta^*) = \pm 0.05$.

In 2-shower events we found it impossible to determine reliably from the photographs which of the two gammas had the higher energy. This meant that there was a two-fold ambiguity in the π^0 direction. Thus, the bisector angle between the 2 showers in the barycentric system was used to approximate the π^0 direction. This approximation proved to be adequate within our statistical accuracy. However, it is not sufficiently accurate for dealing with η^0 decay kinematics.[12]

Uncorrected π^0 angular distributions were determined by adding together the bisector distributions in 2-track events and the gamma distributions in 1-track events. The 2-track events included those 3-track events where one track was deduced to be a neutron recoil. Target full-empty subtractions were made. The full/empty ratio was about 3:1 for the counter data and about 9:1 for the angular-distribution data.

The number of scanned events remaining after full-empty subtractions are given in Table I as a function of incident π^- energy and event complexity. A small correction was made to account for $\pi^0 n$ events where a neutron recoil was observed and one gamma ray was not seen. These are 2-track events but the opening angle generally is greater than ϕ_{max}. Thus, they are excluded by criterion (3) above. We make the reasonable assumption that the ratios of the numbers of events N are $N(2\gamma + n \text{ recoil})/N(2\gamma) = N(1\gamma + n \text{ recoil})/N(1\gamma)$ at each angle. This means that the probability of observing a neutron recoil at a given angle is independent of the probability of <u>not</u> observing a gamma ray. All quantities in the above expression are known except $N(1\gamma + n \text{ recoil})$ which can then be calculated. The numbers of events

calculated were added to the gamma distributions of 1-track events. These were included in the uncorrected π^0 angular distributions.

B. Corrected π^0 Distributions

To more nearly approximate the true π^0 angular distributions, a correction factor $F(T_\pi^{lab}, \theta)$ was calculated. The uncorrected π^0 angular distributions were multiplied by $F(T_\pi^{lab}, \theta)$ to give the true angular distributions.

To calculate this factor, a Monte Carlo computer program was developed. This program used as input an assumed true π^0 angular distribution. It produced as output 1 and 2-track events. Those events satisfying criteria 2 and 3, mentioned in Sec. IIIA., were added together as described above. Then $F(T_\pi^{lab}, \theta)$ was just the ratio of the input π^0 angular distribution to the calculated uncorrected π^0 angular distribution.

We also compared the 1-track distributions predicted by the Monte Carlo calculation directly with the observed 1-shower distribution. They were in reasonable agreement. This reassured us that indeed most of the 1-shower events resulted from the $\pi^0 n$ final state.

The computer program randomized the following:

(1) the point in the LH_2 target where the interactions took place (This automatically builds in an error in the gamma-ray direction, since in reconstruction the event is assumed to originate at the midplane of the target as mentioned above.),

(2) the point in the spark chambers at which the gammas converted (weighted by the pair production cross section),

(3) the detection of the showers (weighted by the detection efficiency of the spark chambers).

Because the true π^0 angular distribution was unknown, the calculation had to be iterated. For the first iteration the observed uncorrected π^0 angular distributions were used as the assumed true distributions. The factor $F(T_\pi^{lab},\theta)$ thus determined was used to correct the observed distributions, and this new true distribution used as input to recalculate $F(T_\pi^{lab},\theta)$. It was found that one iteration was sufficient. As expected, $F(T_\pi^{lab},\theta)$ was always close to one. Figure 5 shows a comparison between the corrected and uncorrected angular distributions at 875 MeV.

C. Detection Efficiency of the Spark Chambers and the $2\pi^0 n$ and $3\pi^0 n$ Background Contributions

We discuss the detection efficiency and the $2\pi^0 n$ and $3\pi^0 n$ background contributions together, since the calculations of these quantities are interdependent.

For the detection efficiency ϵ of the spark chambers, we used

$$\epsilon(E) = 0 \text{ for } E < E_0$$
$$\epsilon(E) = C\left\{1 - \exp\left[-(E - E_0)/\Delta E\right]\right\} \text{for } E \geq E_0 \quad (2)$$

where E is the laboratory energy of the gamma ray, $E_0 = 15$ MeV was calculated theoretically, and $C \leq 1.0$ was a constant. As might be expected, the 1-shower angular distribution was sensitive to the efficiency function $\epsilon(E)$. When we set $C < 0.95$ we found that it was impossible for the 1-shower angular distributions predicted by the Monte Carlo calculation to give a good fit to the observed 1-shower distributions. This finding was insensitive to the ΔE values used. Thus, we had $0.95 \leq C \leq 1.0$.

Three neutral final states contributed significantly to the background; these were $2\pi^0 n$, $3\pi^0 n$, and $\eta^0(\rightarrow 2\gamma)n$. The last of these was easily eliminated because the minimum opening angle for the gamma rays was much

larger than ϕ_{max}. For example, in Fig. 4 the peak at about 140 deg is due to the $\eta^o n$ final state. This reaction was also analyzed in this experiment and as mentioned has been reported elsewhere.[12].

From the various final states we observed events with 1 to 6 showers. Very few events were observed with more than 6 showers. The relative numbers of 1- to 6-shower events depend on the cross sections for the $\pi^o n$, $2\pi^o n$, and $3\pi^o n$ final states and the spark-chamber detection efficiency. [We exclude $\eta^o(\rightarrow 2\gamma)n$ final states as described above.] We selected two groups of the 2-shower events: those that satisfied criterion (3) in Sec. IIIA above, and those in which the gamma opening angle was greater than ϕ_{max} but less than ϕ_{min} - 10 deg, where ϕ_{min} is the minimum opening angle for the $\eta^o(\rightarrow 2\gamma)$ final state. This then gave seven measured quantities depending on three differential cross sections and the spark-chamber detection efficiency. The uncorrected π^o angular distribution was used for the $\pi^o n$ final state. The distributions of π^o's in $2\pi^o n$ and $3\pi^o n$ final states were assumed to be given by isotropic invariant phase space. Thus the energy and the angular distributions in the three final states were assumed to be known. Only the total cross sections were unknown. These total cross sections were calculated from

$$\sigma_j = \frac{N_j^{cal}}{N} \quad \sigma_{neut} ,$$

where j(1, 2 and 3) represents $\pi^o n$, $2\pi^o n$ and $3\pi^o n$ final states, σ_{neut} is total neutral cross sections, N is total number of events, and N_j^{cal} is the number of events in class j calculated by a least squares fit from the number of observed 1 to 6 shower events (with the 2-shower events divided into two categories as mentioned above) and the efficiency

$\epsilon(E)$.

We found that the factor $F(T_\pi^{lab},\theta_\pi)$ did not depend significantly on C provided $0.95 \leq C \leq 1.0$. In the Monte Carlo calculation of $F(T_\pi^{lab},\theta_\pi)$ we then set C = 1.0. In the determination of the total cross sections we used C = 0.975.

The final values of ΔE varied somewhat from energy to energy. This was due to variable running conditions. Furthermore, the values of ΔE for the Hawaii scanning were higher than those for the Berkeley scanning, due to the stricter minimum track requirement used by the Hawaii group, as mentioned in Sec. IIIA. With C = 0.975, ΔE for the Berkeley group ranged from 60 to 70 MeV and for the Hawaii group from 75 to 85 MeV.

The contribution to the 1- and 2-shower events (as defined in IIIA) due to $2\pi^o n$ final states ranged from 2% to 4%. For $3\pi^o n$ final states, in most cases this contribution was less than 1.5%. The contributions of these backgrounds to the π^o angular distribution are essentially flat in $\cos\theta_{\pi^o}$, they are smaller than our experimental errors. No subtraction for these backgrounds was made for the π^o angular distributions presented in Sec. IVB. The opening angle curve shown in Fig. 4 resulted from a fit to $\pi^o n + 2\pi^o n$ final states at 655 MeV, and the dotted curve is the small contribution due to $2\pi^o n$ events alone. In this case, the contribution of the $3\pi^o n$ final state was negligible.

D. Errors

In addition to the statistical error, there were several other important sources of error. In this section we discuss their effect on each of the various results of this experiment.

1. Relative Errors in the $\pi^o n$ Angular Distribution

Two significant sources of error that affected the angular distributions were (a) the statistical error in the Monte Carlo determination of $F(T_\pi^{lab},\theta)$ and (b) the uncertainty in the spark-chamber efficiency. The first uncertainty was due to the use of only a finite number of Monte Carlo events. At each energy this amounted to about 5000 events. The second uncertainty had two sources: (1) uncertainty in the energy dependence of the efficiency $\epsilon(E)$ in expression (2), and (2) anisotropy of the efficiency. The energy dependence was determined by the two

parameters C and ΔE. As previously noted, $F(T_\pi^{lab}, \theta_\pi)$ did not depend on C for $0.95 \leq C \leq 1.0$. It did however depend on ΔE. This parameter was allowed to vary between limits consistent with the relative numbers of 1- to 6-shower events. The effect on $F(T_\pi^{lab}, \theta_\pi)$ was noted, and an error estimated.

An angular asymmetry was also observed for the efficiency. This was due to the cubic geometry of the spark chambers. The efficiency was varied within the limits of the observed asymmetry. The effect on the calculation of $F(T_\pi^{lab}, \theta_\pi)$ was again noted and an error estimated.

The above uncertainties resulted in an additional error about equal to the statistical error. Both are included in the relative errors in the results of Tables II and III.

Other uncertainties investigated were due to (1) momentum spread of the π beam, (2) finite size of the target, and (3) errors in track measurements. These were all found to be negligible.

2. Normalization of the Total Neutrals Cross Section

Three uncertainties contributed to the normalization error of the total neutrals cross section:

(a) uncertainty in pion flux (± 2%),

(b) uncertainty in LH_2 density (± 3%),

(c) fluctuations in the efficiency of the anticounters A_{1-9} for detecting charged particles. This manifested itself by a lack of reproducibility of different runs at each energy. It varied from ±4% to ±8% and was the main source of error in the cross section for $\pi^- p \rightarrow$ neutrals.

These uncertainties are included in the results of Table IV.

3. Total Cross Section for the $\pi^0 n$ Final State

The angular distributions were fit to a sum of Legendre polynomials,

$$\frac{d\sigma}{d\Omega} = \sum C_\ell P_\ell(\cos\theta),$$

where $P_\ell(\cos\theta)$ is the Legendre polynomial of order ℓ, and θ is the c.m. angle of the pion. The relative error in the total cross section for the $\pi^0 n$ final state was then determined from the error in C_0,

$$\frac{\Delta\sigma_{\pi^0 n}}{\sigma_{\pi^0 n}} = \frac{\Delta C_0}{C_0} .$$

The error in C_0 of course includes the statistical error. The total cross section was normalized to the total neutrals cross section. Thus, the final errors tabulated in Table II include both the above-determined relative error and the error in the total neutrals cross section.

4. Cross Sections for the $2\pi^0 n$ and $3\pi^0 n$ Final States

In contrast to $F(T_\pi^{lab}, \theta_\pi)$ the cross sections for the $2\pi^0 n$ and $3\pi^0 n$ final states were quite sensitive to the value of C. We set $C = 0.975 \pm 0.025$. This is consistent with the previously established limits on C. The errors estimated for ΔE also affected these cross sections. With few exceptions the estimated errors in C and ΔE resulted in the following range of percentage errors on the cross sections at various energies:

	C	ΔE
$\Delta\sigma(\pi^- p \to \pi^0 n)$	$\sim \pm 2\%$	$\sim \pm 1\%$
$\Delta\sigma(\pi^- p \to 2\pi^0 n)$	$\pm 4\%$ to $\pm 9\%$	$\pm 4\%$ to $\pm 16\%$
$\Delta\sigma(\pi^- p \to 3\pi^0 n)$	$\pm 7\%$ to $\pm 17\%$	$\pm 11\%$ to $\pm 24\%$.

Fluctuations in the scanning efficiency for counting 1- to 6-shower events were estimated by multiple scanning of selected portions of the film. From these fluctuations an error was estimated. This error was added to the statistical error in the numbers of 1- to 6-shower events.

The resulting sum was included in the least-squares analysis. The added uncertainty due to scanning-efficiency fluctuations were as follows:

Number of showers	Fluctuation error (%)
1	±4.5
2	±3.5
3	±2.5
4	±7.5
5	±11.5
6	±25.0

These errors were then included in the $2\pi^0 n$ and $3\pi^0 n$ cross sections.

These cross sections were also normalized to the total-neutrals cross section. The final errors shown in Table IV outside the parentheses, include both the errors discussed in this section and the error in the total-neutrals cross section. Errors for $2\pi^0 n$ and $3\pi^0 n$ cross section, in the parenthesis, do not include the uncertainty due to the choice of C and ΔE values. They could be taken as the relative errors for the shape of the curves $\sigma_{2\pi^0}$ vs T_π^{lab} and $\sigma_{3\pi^0}$ vs T_π^{lab}.

IV. RESULTS

A. Total Cross Section

We determined the cross section for $\pi^- p \rightarrow$ all neutrals electronically. This cross section was calculated from the ratio (neutral counts)/(monitor counts). These numbers were recorded by scalers on the outputs of coincidence units W_1 and W_2 in Fig. 2. In the actual calculation the number of neutral counts was reduced slightly to correct for the inefficiency of the anticounter. This inefficiency was determined by noting the number of events photographed in which charged particles were produced in the LH_2 target. The results are shown in Table IV. Figure 6 displays our results and those of two other experiments.[10, 15]

The relative cross sections for the three final states $\pi^0 n$, $2\pi^0 n$, and $3\pi^0 n$ were determined by a least-squares fit to the relative numbers of 1- to 6-shower events at each energy as described in Sec. IIIC. These were normalized to the total neutral cross section. The resulting absolute cross sections are listed in Table IV.[16] They are plotted in Figs. 7 and 8, along with the results of Refs. 10 and 15.

B. Differential Cross Section

The differential cross sections were taken from the corrected π^0 angular distributions for the $\pi^0 n$ final state.

In spite of the somewhat different shower criteria, the distributions obtained by the Berkeley scanning and the Hawaii scanning are in very good agreement. These distributions are normalized to the total cross sections of Table IV. The differential cross sections are tabulated in Table II and plotted in Fig. 9. The solid curves are least-squares

fits of our data to sums of Legendre polynomials. The series for each energy are terminated at the smallest value of ℓ_{max} for which the statistical fit to the data has (a) the $\sqrt{\chi^2/d}$ value close to unity, where d is the degree of freedom and (b) no further appreciable change in the value of $\sqrt{\chi^2/d}$ for greater values of ℓ_{max}. The coefficients are listed in Table III. They are plotted in Fig. 10, along with the results of one other experiment.[17]

The dotted curves of Fig. 9 are the results of least-squares fits to the data of Ref. 10 at comparable energies. Agreement is good only at 533 and 875 MeV. At 655 MeV agreement is poor in the forward direction, where $\cos\theta_\pi > 0.4$. The most significant disagreement is at 975 and 1117 MeV in the backward direction. At 875 MeV both experiments see a peak at $\cos\theta_\pi = -0.8$ and a subsequent fall off to nearly zero at $\cos\theta_\pi = -1$. This is also seen in π^-p elastic scattering and is characteristic of the T = 1/2 resonance at 900 MeV.[3] At higher energies our results show a decline in the peak at $\cos\theta_\pi = -0.8$ and a <u>rise</u> in the differential cross section at $\cos\theta = -1$. This latter feature is also seen in π^+p elastic scattering and is characteristic of the T = 3/2 resonance at 1354 MeV.[2] As seen in Fig. 9 the latter effect is much reduced in the results of Ref. 10, in spite of the fact that the results of Ref. 10 are for energies slightly <u>higher</u> than ours.

C. Forward and Backward Differential Cross Section

From the coefficients of Table III we have calculated the differential cross section at 0 and 180 deg. The results are listed in Table V. The values at 0 deg are plotted in Fig. 11 along with the results of three other experiments.[6,10,18] The curve is the result calculated from dispersion theory.[19]

V. DISCUSSION

A. T = 1/2 Scattering

From the charge-exchange coefficients in Table III and the coefficients from $\pi^{\pm}p$ elastic scattering[1-4] we have calculated the coefficients C_ℓ for scattering in the T = 1/2 state in the expression

$$\frac{d\sigma}{d\Omega}(T = 1/2) = \sum C_\ell P_\ell \ (\cos\theta) ,$$

where $P_\ell(\cos\theta)$ is the Legendre polynomial of order ℓ, and θ is the pion c.m. angle. These coefficients along with $\sigma(T = 1/2)$ are tabulated in Table VI. The coefficients are plotted in Fig. 12. The energies are slightly different from the energies of this experiment. This resulted from averaging data at slightly different energies from different experiments.

B. 600-MeV Resonance

From Fig. 12 we see that in this energy region there are significant peaks in C_0, C_1, and C_2. Furthermore, coefficients C_ℓ, for $\ell \geqslant 3$ are small. This implies the resonance can involve only states with $J \leqslant 3/2$. Since we have $C_1 > C_3$, at least one J = 1/2 amplitude is important. (If only J = 3/2 amplitudes are nonzero, then we have $C_1 = C_3/9$.)

C. 900-MeV Resonance

In this energy region C_5 shows a sharp peak. Since C_ℓ for $\ell \geqslant 6$ are very small, C_5 is determined entirely by a $D_{15}F_{15}$ interference term. Thus either the D_{15} or the F_{15} amplitudes or both must be rapidly varying in this energy region. This interference is entirely in the T = 1/2 state.

D. Phase-Shift Analyses

Complete sets of phase shifts from 300 to 700 MeV have been published by several groups[20-23] and from 300 to 1000 MeV by two groups.[24,25] There is also another unpublished set from 700 to 1000 MeV.[26] With one exception,[23,26] the various sets of phase shifts are in qualitative agreement. However, there are quantitative disagreements among all the various sets. This is because the experimental quantitities are quadratic in the partial-wave amplitudes which in turn are periodic in the phase shifts. Only by greatly overdetermining the expressions relating experiment to the phase shifts can one hope to arrive at a unique set. This was a major motivation for this experiment. Although charge-exchange differential-cross-section data have certainly helped, and in fact are required, this goal has still not been achieved. Further experiments are necessary. It has been shown that the various sets of phase shifts predict quite different recoil-neutron polarization distributions in charge-exchange near the 600-MeV resonance.[27] This, then, is an important experiment.

Finally, we show curves of the C_ℓ in Fig. 12 predicted by two sets of phase shifts.[23,24,26] Preliminary forms of our data were included in the least-squares analysis, resulting in these two sets. It is not surprising, then, that the fit is good. One of these sets of phase shifts is the one in serious qualitative disagreement with all the others.[23,26] This shows that more-precise charge-exchange differential-cross-section data would not be nearly as useful as recoil-neutron polarization data.

ACKNOWLEDGMENTS

We thank our scanning and measuring groups for their continued high-quality efforts which facilitated the successful completion of this experiment. We also thank the Bevatron staff under the direction of Dr. E. J. Lofgren and the staff of the Computer Center for their excellent cooperation.

Table I. Number of events after full-empty subtractions.

$T_{\pi^-}^{lab}$ (MeV)	Shower number					
	1	2	3	4	5	6
500	4563	8203	1240	524	59	6
533	2814	4966	768	321	31	4
592	1885	4466	752	537	133	41
655	2371	6730	1755	1215	382	112
704	2768	6373	2215	1471	384	126
875	1910	6107	2027	1415	360	97
975	1927	4841	1662	1138	293	90
1117	1172	4461	1893	1591	580	233
1300	1473	6486	2702	2471	802	389

Table II. Differential cross sections for $\pi^- p \rightarrow \pi^0 n$.

$\cos\theta_\pi$	$d\sigma/d\Omega$ (mb/sr)								
	T_π^{lab}(MeV) = 500	533	592	655	704	875	975	1117	1300
0.950	3.700±.309	4.086±.314	3.219±.263	1.484±.115	1.285±.116	2.075±.140	0.822±.058	0.414±.039	0.386±.038
0.850	2.796±.220	2.794±.226	2.106±.182	1.109±.079	0.677±.061	0.946±.071	0.323±.027	0.283±.031	0.378±.026
0.750	1.847±.146	1.817±.150	1.611±.129	0.681±.050	0.418±.035	0.438±.042	0.179±.019	0.195±.019	0.227±.018
0.650	1.403±.101	1.453±.120	1.088±.098	0.516±.046	0.264±.031	0.229±.028	0.141±.017	0.146±.018	0.122±.014
0.550	1.018±.072	0.976±.080	0.886±.075	0.466±.043	0.249±.024	0.175±.026	0.220±.028	0.207±.025	0.112±.015
0.450	0.707±.047	0.646±.058	0.634±.059	0.345±.035	0.195±.025	0.229±.034	0.309±.033	0.169±.021	0.102±.011
0.350	0.644±.046	0.533±.054	0.478±.057	0.348±.037	0.270±.029	0.292±.040	0.327±.029	0.205±.025	0.158±.016
0.250	0.403±.036	0.347±.045	0.399±.045	0.315±.026	0.217±.026	0.276±.038	0.302±.031	0.169±.021	0.148±.018
0.150	0.405±.033	0.331±.039	0.233±.039	0.266±.031	0.180±.022	0.240±.038	0.186±.018	0.099±.018	0.103±.013
0.050	0.315±.042	0.296±.048	0.210±.037	0.185±.027	0.157±.019	0.204±.035	0.131±.017	0.088±.016	0.108±.014
-0.050	0.321±.030	0.279±.042	0.228±.037	0.159±.022	0.112±.014	0.132±.025	0.086±.013	0.044±.012	0.094±.010
-0.150	0.239±.024	0.204±.028	0.160±.028	0.148±.023	0.139±.018	0.083±.021	0.068±.011	0.036±.007	0.096±.010
-0.250	0.271±.038	0.248±.044	0.170±.042	0.119±.015	0.169±.018	0.073±.019	0.055±.009	0.073±.010	0.099±.010
-0.350	0.228±.032	0.140±.026	0.109±.025	0.180±.025	0.256±.026	0.191±.028	0.117±.018	0.111±.017	0.119±.011
-0.450	0.170±.026	0.074±.026	0.115±.029	0.315±.041	0.380±.037	0.438±.049	0.183±.023	0.180±.022	0.156±.016
-0.550	0.150±.024	0.129±.033	0.130±.034	0.272±.050	0.428±.048	0.592±.062	0.295±.032	0.194±.023	0.189±.019
-0.650	0.126±.026	0.108±.030	0.177±.036	0.444±.067	0.578±.065	1.036±.041	0.393±.041	0.210±.025	0.220±.025
-0.750	0.088±.028	0.126±.035	0.182±.032	0.503±.061	0.723±.072	1.253±.092	0.430±.039	0.148±.021	0.136±.019
-0.850	0.079±.022	0.172±.057	0.311±.047	0.449±.041	0.585±.063	1.068±.070	0.332±.029	0.141±.020	0.125±.015
-0.950	0.178±.052	0.250±.061	0.431±.066	0.322±.067	0.355±.041	0.597±.090	0.432±.042	0.327±.030	0.281±.022
Corrected number of events	8222	5364	3864	5153	5202	5049	4037	3179	5319
Normal error, %	5.5	5.5	5.5	5.5	5.5	5.5	9.5	8.3	8.4

Table III. Coefficients in Legendre polynomial expansion

$$\frac{d\sigma}{d\Omega} = \sum C_\ell P_\ell (\cos\theta) \text{ in mb/sr}$$

for $\pi^- p \rightarrow \pi^0 n$.[a]

	Coefficients								
	T_π^{lab}(MeV) = 500	533	592	655	704	875	975	1117	1300
C_0	0.747±.019	0.738±.022	0.638±.015	0.429±.010	0.381±.009	0.528±.011	0.263±.008	0.172±.004	0.167±.005
C_1	1.302±.045	1.307±.053	0.988±.035	0.329±.023	0.056±.020	0.036±.024	0.047±.017	0.035±.008	0.038±.011
C_2	1.106±.057	1.265±.068	1.063±.045	0.543±.029	0.479±.026	0.887±.031	0.297±.022	0.171±.011	0.154±.014
C_3	0.677±.049	0.682±.058	0.424±.040	0.293±.037	0.352±.029	0.572±.038	0.088±.028	0.005±.014	0.056±.018
C_4	0.313±.039	0.392±.049	0.265±.036	0.056±.034	-0.006±.026	0.162±.033	0.128±.032	0.048±.015	0.068±.019
C_5	---	---	---	0.290±.036	0.369±.031	0.834±.038	0.350±.029	0.026±.017	-0.029±.021
C_6	---	---	---	---	---	---	0.182±.033	0.155±.016	0.041±.019
C_7	---	---	---	---	---	---	---	-0.114±.018	-0.141±.022
Normal error, %	5.5	5.5	5.5	5.5	5.5	5.5	9.5	8.3	8.4

[a]The errors come from the diagonal elements of the error matrices. Normalization error not included.

Table IV. Cross sections for various neutral final states.[a]

T_π^{lab} (MeV)	$\sigma_{neut.}$ (mb)	$\sigma_{\pi^0 n}$ (mb)	$\sigma_{2\pi^0 n}$ (mb)	$\sigma_{3\pi^0 n}$ (mb)
500	12.16±0.67	9.48±0.57	2.12±0.28(0.21)	0.30±0.19(0.10)
533	11.86±0.65	9.43±0.59	2.36±0.30(0.23)	0.20±0.14(0.07)
592	11.89±0.65	8.09±0.48	1.79±0.40(0.24)	1.16±0.43(0.21)
614	11.27±0.62			
655	9.69±0.53	5.42±0.32	2.03±0.38(0.20)	1.28±0.41(0.18)
670	9.72±0.53			
704	9.54±0.52	4.80±0.29	1.94±0.52(0.34)	1.51±0.49(0.29)
726	8.59±0.47			
765	8.90±0.49			
786	9.25±0.51			
805	10.16±0.56			
837	11.37±0.63			
875	11.35±0.62	6.64±0.39	3.06±0.37(0.28)	1.11±0.31(0.18)
914	9.29±0.56			
955	7.40±0.48			
975	6.58±0.44	3.35±0.33	1.82±0.37(0.26)	0.94±0.34(0.24)
1117	5.08±0.42	2.16±0.19	1.45±0.29(0.18)	0.92±0.21(0.15)
1300	4.62±0.39	2.11±0.19	1.33±0.26(0.16)	0.70±0.17(0.12)

[a]Errors outside the parentheses are absolute errors. Errors within the parentheses for $\sigma_{2\pi^0 n}$ and $\sigma_{3\pi^0 n}$ are the relative errors. (See Sec. D3.) See also footnote 16.

Table V. Forward and backward differential cross sections for $\pi^- p \rightarrow \pi^0 n$ calculated from the coefficients of Table IV.[a]

T_π^{lab} (MeV)	$\frac{d\sigma}{d\Omega}$ (0 deg) (mb/sr)	$\frac{d\sigma}{d\Omega}$ (180 deg) (mb/sr)
500	4.145±0.297	0.187±0.044
533	4.384±0.327	0.405±0.070
592	3.377±0.237	0.554±0.059
655	1.941±0.159	0.116±0.079
704	1.630±0.137	0.078±0.054
875	3.020±0.202	0.134±0.095
975	1.355±0.166	0.384±0.095
1117	0.498±0.072	0.593±0.069
1300	0.354±0.089	0.505±0.069

[a]Normalization error included.

Table VI. Coefficients in the Legendre polynomial expansion

$$\frac{1}{\lambda^2}\frac{d\sigma}{d\Omega} = \sum C_\ell P_\ell(\cos\theta)$$

for $\pi N \rightarrow \pi N$ in isospin state $T = 1/2$.[a]

	Coefficients								
	T_π^{lab} (MeV) = 495	533	585	650	700	873	985	1117	1300
C_0	0.820±.034	1.100±.042	1.444±.045	1.345±.038	1.335±.031	2.833±.072	2.044±.047	1.287±.046	1.230±.054
C_1	0.863±.073	1.354±.095	1.904±.105	1.622±.084	1.208±.059	2.218±.159	2.629±.078	2.119±.106	2.368±.117
C_2	1.099±.089	1.767±.115	2.396±.135	1.981±.117	1.987±.082	6.504±.228	5.082±.119	3.135±.149	2.989±.160
C_3	0.282±.083	0.091±.097	0.428±.121	0.703±.121	1.057±.082	5.742±.231	4.629±.118	2.984±.165	3.003±.167
C_4	0.343±.059	0.397±.068	0.363±.099	-0.065±.097	0.120±.071	2.464±.215	2.651±.118	1.696±.159	2.077±.157
C_5	0.060±.039	0.068±.052	0.118±.093	0.343±.074	0.776±.065	3.468±.174	2.480±.106	1.163±.136	1.302±.146
C_6	-	-	0.091±.088	-	0.261±.057	0.163±.145	0.070±.096	-0.127±.101	-0.035±.126
C_7	-	-	-	-	-	0.050±.039	0.065±.035	-0.028±.084	0.129±.130
λ^2(mb)	2.413	2.209	1.977	1.744	1.597	1.231	1.069	0.924	0.772
$\sigma_t(T=\frac{1}{2})$ (mb)	24.9±1.0	30.5±1.2	35.9±1.1	29.5±0.8	26.8±0.6	43.8±1.1	27.5±0.6	14.9±0.5	11.9±0.5
$\pi^\pm p$ data used	Ref. 1	Ref. 2, 3	Ref. 2, 3	Ref. 1	Ref. 2, 3	Ref. 2, 3	Ref. 2, 3	Ref. 4	Ref. 2, 4

[a]The errors come from the diagonal elements of the error matrices. Normalization errors included.

FOOTNOTES AND REFERENCES

*This work was done under the auspices of the United States Atomic Energy Commission.

†Present address: Department of Physics, University of Notre Dame, Notre Dame, Indiana.

‡Present address: Department of Physics, Tufts University, Medford, Massachusetts.

1. P. M. Ogden, D. E. Hagge, J. A. Helland, M. Banner, J. F. Detoeuf, and J. Teiger, Phys. Rev. 137, B1115 (1965).

2. J. A. Helland, T. J. Devlin, D. E. Hagge, M. J. Longo, B. J. Moyer, and C. D. Wood, Phys. Rev. 134, B1062 (1964).

3. J. A. Helland, C. D. Wood, T. J. Devlin, D. E. Hagge, M. J. Longo, B. J. Moyer, and V. Perez-Mendez, Phys. Rev. 134, B1079 (1964).

4. P. J. Duke, D. P. Jones, M. A. R. Kemp, P. G. Murphy, J. D. Prentice, J. J. Thresher, H. H. Atkinson, C. R. Cox, and K. S. Heard, Phys. Rev. Letters 15, 468 (1965).

5. R. D. Eandi, T. J. Devlin, R. W. Kenney, P. G. McManigal, and B. J. Moyer, Phys. Rev. 136, B536 (1964).

6. P. Borgeaud, C. Bruneton, Y. Ducros, P. Falk-Vairant, O. Guisan, J. Movchet, P. Sonderegger, A. Stirling, M. Yvert, A. Tran Ha, and S. D. Warshaw, Phys. Letters 10, 134 (1964).

7. (a) A. Weinberg, A. E. Brenner, and K. Strauch, Phys. Rev. Letters 8, 70 (1962); (b) Brandeis-Brown-Harvard-MIT-Padova Collaboration, in 1962 Annual International Conference on High Energy Physics at CERN, edited by B. Ferretti (CERN Scientific Information Service, Geneva, 1962).

8. A Bigi, R. Carrara, and D. Zanello, Nuovo Cimento, Series 10, 34, 878 (1964).

9. A. Muller, E. Pauli, R. Barloutaud, J. Meyer, M. Beneventano, G. Gialanella, and L. Paoluzi, Phys. Letters 10, 349 (1964).

10. Brandeis-Brown-Harvard-MIT-Padova Collaboration, Phys. Rev. Letters 13, 558 (1964); L. Guerriero, Proc. Royal Soc. (London) 289, 471 (1966).

11. Preliminary results of this experiment have been previously reported. See C. B. Chiu, R. J. Cence, R. D. Eandi, R. W. Kenney, B. J. Moyer, J. A. Poirier, V. Z. Peterson, and W. B. Richards, Bull. Am. Phys. Soc. 8, 603 (1963); R. W. Kenney, C. B. Chiu, R. D. Eandi, B. J. Moyer, J. A. Poirier, W. B. Richards, R. J. Cence, V. Z. Peterson, and V. J. Stenger, Bull. Am. Phys. Soc. 9, 409 (1964).

12. W. Bruce Richards, Charles B. Chiu, Richard D. Eandi, A. Carl Helmholz, Robert W. Kenney, Burton J. Moyer, John A. Poirier, Robert J. Cence, Vincent Z. Peterson, Narender K. Sehgal, and Victor J. Stenger, Phys. Rev. Letters 16, 1221 (1966).

13. For more details, see C. B. Chiu, Pion-Proton Charge-Exchange Scattering, 500 to 1300 MeV, Lawrence Radiation Laboratory report UCRL-16209 (Ph. D. Thesis), November 1965 (unpublished).

14. Janos Kirz, Lawrence Radiation Laboratory, Berkeley, private communication, 1965.

15. J. C. Brisson, P. Falk-Vairant, J. P.Merlo, P. Sonderegger, R. Turlay, and G. Valladas, in Proceedings of the Aix-en-Provence International Conference on Elementary Particles, 1961 (CEN, Saclay, 1961) Vol. 1, p. 45.

16. The final cross section values presented here (especially for $2\pi^0 n$ and $3\pi^0 n$ final states) differ from the preliminary values reported to the Dubna Conference. (Proceedings of the XII Conference on High Energy Physics, Dubna, 1964, Vol. I, p. 30). As stated in the Dubna report, the preliminary values for $(2\pi^0 n)$ and $(3\pi^0 n)$ were just the cross sections for (3- and 4-shower) and (5- and 6-shower) events respectively. The final values based on the improved statistics and extensive Monte Carlo studies of the energy response of our spark chamber system (see Sec. IIIC) take into account the considerable number of $(3\pi^0 n)$ events which are observed as $\leq$ 4-showers, etc. For example, at $T_\pi^{Lab} = 875$ MeV, only one-third of $(3\pi^0 n)$ events occur as 5- or 6-showers, although 3/4 of $(2\pi^0 n)$ events occur as 3- or 4-showers. A Least-squares fitting of the $\pi^0 n$, $2\pi^0 n$ and $3\pi^0 n$ total cross sections to the observed shower-number distribution was used. As for the $\pi^0 n$ and total neutral cross sections, the Dubna and final values are in reasonable agreement at all but one point (i.e., for the $\pi^0 n$ cross section at 975 MeV). For the total neutral cross sections, errors displayed in the Dubna report included only the statistical errors.

17. D. L. Lind, B. C. Barish, R. J. Kurz, P. M. Ogden, and V. Perez-Mendez, Phys. Rev. 138, B1509 (1965).

18. W. S. Risk and E. Kleckner, Bull. Am. Phys. Soc. Series II, 11, 36, (1966). Winthrop S. Risk, Measurement of the Differential Cross Section at 0° for the Reaction $\pi^- p \rightarrow \pi^0 n$ (Ph. D. Thesis), Princeton University, 1965 (unpublished).

19. G. Höhler, J. Baacke, and R. Strauss, Phys. Letters 21, 223 (1966).

20. L. D. Roper, R. M. Wright, and B. T. Feld, Phys.Rev. 138, B190 (1965).

21. B. H. Bransden, P. J. O'Donnell, and R. G. Moorhouse, Phys. Letters 11, 339 (1964).

22. P. Auvil, C. Lovelace, A. Donnachie, and A. T. Lea, Phys. Letters 12, 76 (1964).

23. R. J. Cence, Phys. Letters 20, 306 (1966).

24. P. Bareyre, C. Bricman, A. V. Stirling, and G. Villet, Phys. Letters 18, 342 (1965).

25. B. H. Bransden, P. J. O'Donnell, and R. G. Moorhouse, Phys. Letters 19, 420 (1965).

26. R. J. Cence (University of Hawaii), private communication.

27. R. J. Cence, University of Hawaii report HEPG-3-65, June 1965.

FIGURE LEGENDS

Fig. 1. Plan view of the experimental arrangement.

Fig. 2. Block diagram of the electronics.

Fig. 3. Spark chamber and LH_2 target assembly.

Fig. 4. The c.m. opening-angle distribution of the 2-shower events for $T_\pi^{lab} = 655$ MeV. The curve is a fit to the 2-shower events produced by $\pi^0 n + 2\pi^0 n$ final states as determined by a Monte Carlo calculation. The dotted curve is due to the contribution of $2\pi^0 n$ alone.

Fig. 5. The c.m. uncorrected π^0 distribution (curve A) and the corrected π^0 distribution (curve B) at $T_\pi^{lab} = 875$ MeV.

Fig. 6. Total cross section for $\pi^- p \to$ neutrals. □ Ref. 10; △ Ref. 15; ⊙ this experiment.

Fig. 7. Total cross section for $\pi^- p \to \pi^0 n$. □ Ref. 10; △ Ref. 15; ⊙ this experiment.

Fig. 8. Cross sections for $\pi^- p \to 2\pi^0 + n$ and $3\pi^0 + n$. □ Ref. 10; ⊙ this experiment. Error bars plotted for the data points of this experiment are absolute errors.

Fig. 9. The c.m. π^0 angular distributions in $\pi^- p \to \pi^0 n$. The solid curves are least-squares fits to the results of this experiment. The dotted curves are the fits to the results of Ref. 10 at nearby energies. Errors do not include normalization uncertainty.

Fig. 10. Coefficients C_ℓ in the expansion

$$\frac{d\sigma}{d\Omega}(\pi^- p \to \pi^0 n) = \sum_\ell C_\ell P_\ell(\cos\theta),$$

where $P_\ell(\cos\theta)$ is the Legendre-polynomial order ℓ, and θ is the c.m. pion angle. △ Ref. 17; ⊙ this experiment.

Errors include the normalization error. The curves were hand-drawn to guide the eye.

Fig. 11. Differential cross section at $\theta_{c.m.} = 0$ deg for $\pi^- p \rightarrow \pi^0 n$. ▽ Ref. 6; △ Ref. 10; □ Ref. 18; ⊗ this experiment. The curve is the result of a dispersion theoretical calculation.[19]

Fig. 12. Coefficients in the expansion

$$\frac{d\sigma}{d\Omega}(T = 1/2) = \sum_{\ell} C_{\ell} P_{\ell}(\cos\theta),$$

where $(d\sigma/d\Omega)(T = 1/2)$ is the differential cross section for $\pi N \rightarrow \pi N$ in the isospin state $T = 1/2$.

⊗ this experiment. The solid curves are predicted by the phase shifts of Ref. 24 and the dashed curves by the phase shifts of Refs. 23 and 26.

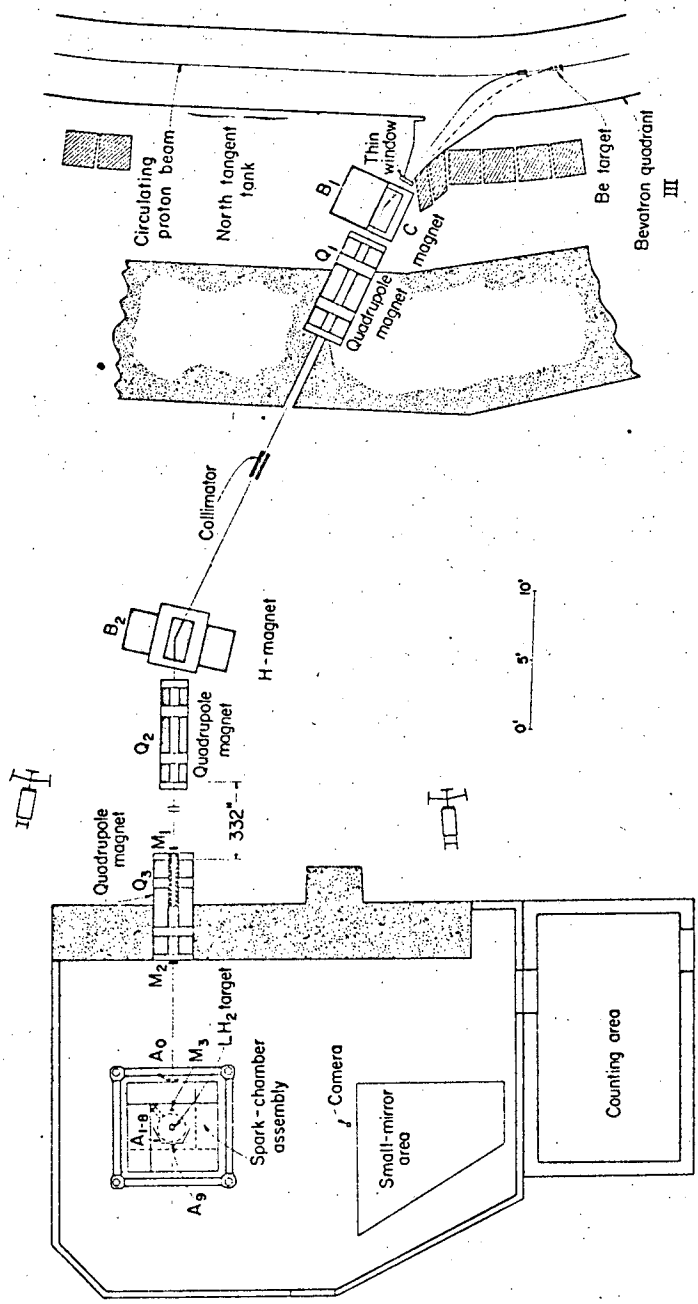

MUB-7092

Fig. 1

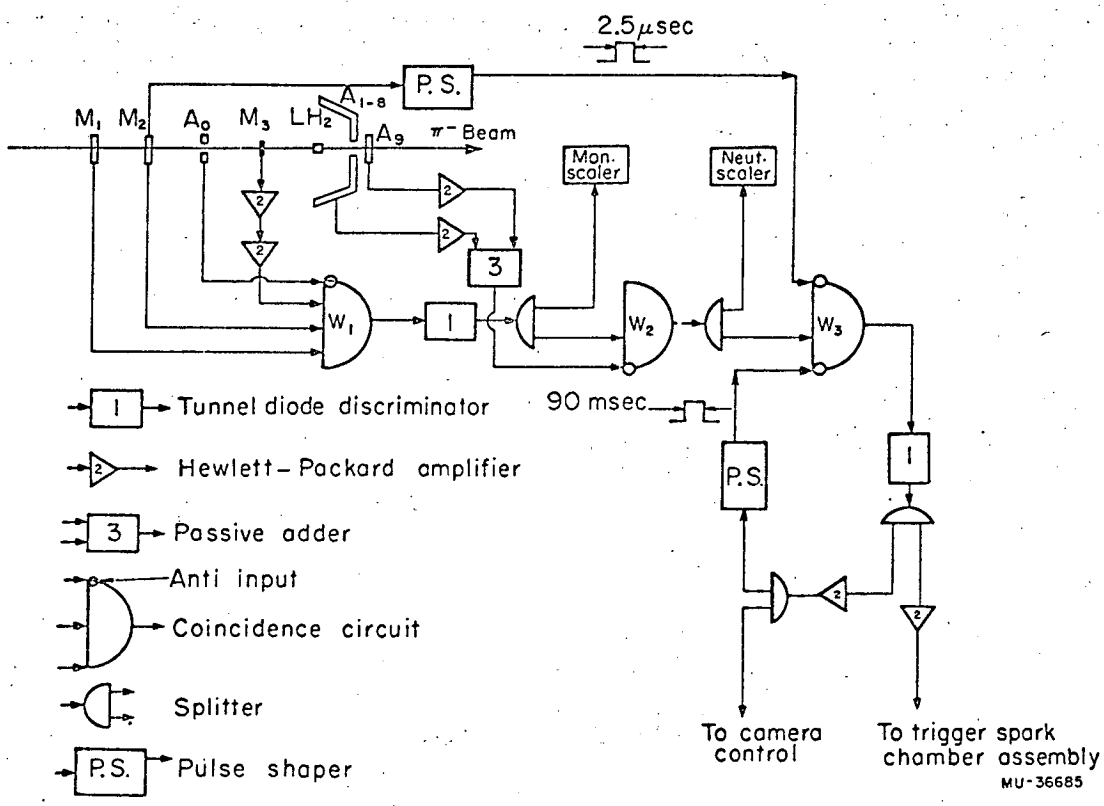
2.5μsec
P.S.
M1
M2
A0
M3
LH2
A1-8
A9
π⁻ Beam
Mon. scaler
Neut. scaler
3
W1
1
W2
W3
90 msec
P.S.
1
To camera control
To trigger spark chamber assembly
MU-36685
Tunnel diode discriminator
Hewlett-Packard amplifier
Passive adder
Anti input
Coincidence circuit
Splitter
Pulse shaper

Fig. 2

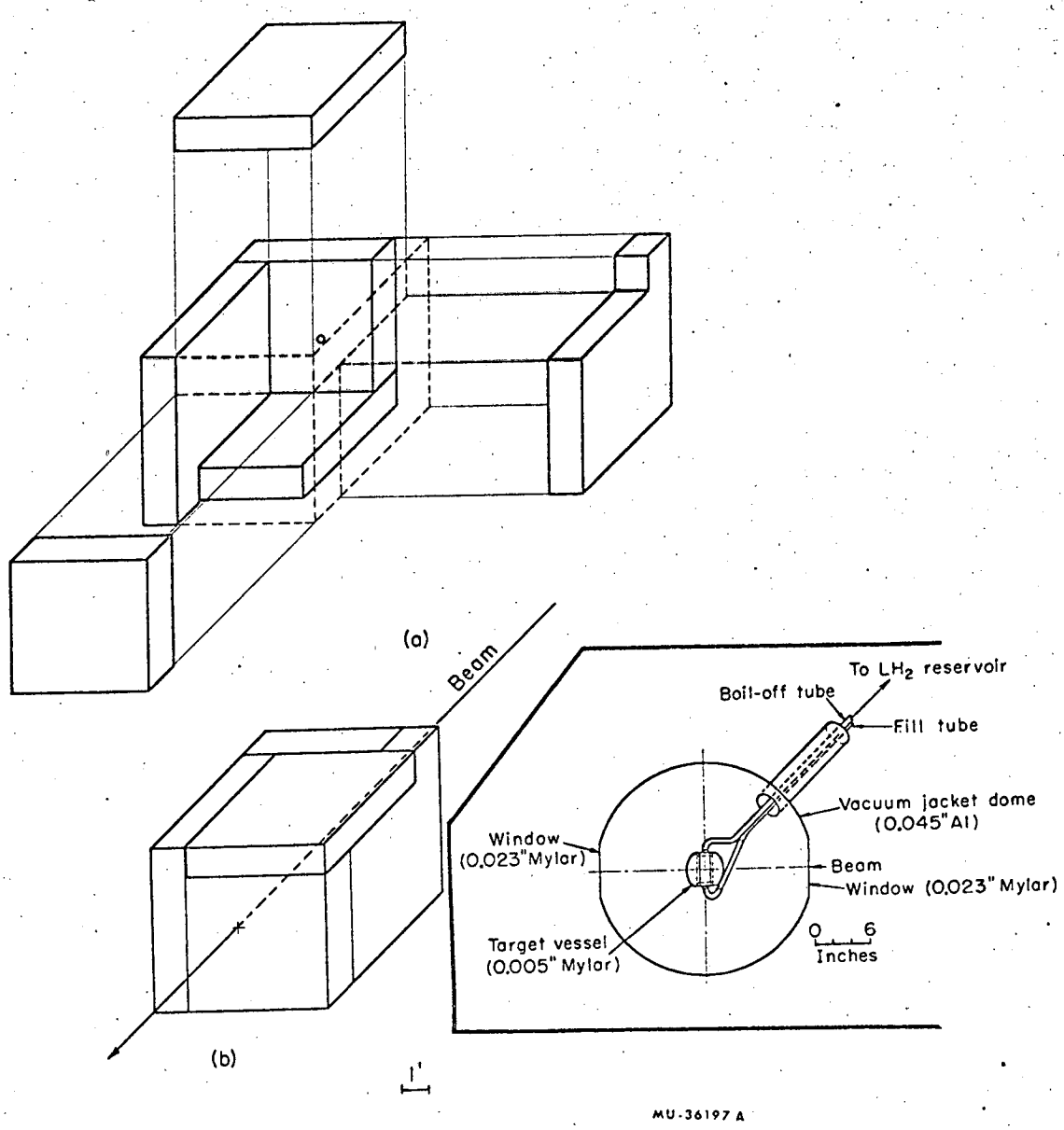
(a)
Beam
(b)
1'
To LH_2 reservoir
Boil-off tube
Fill tube
Vacuum jacket dome
(0.045" Al)
Window
(0.023" Mylar)
Beam
Window (0.023" Mylar)
Target vessel
(0.005" Mylar)
0 6
Inches
MU-36197 A

Fig. 3

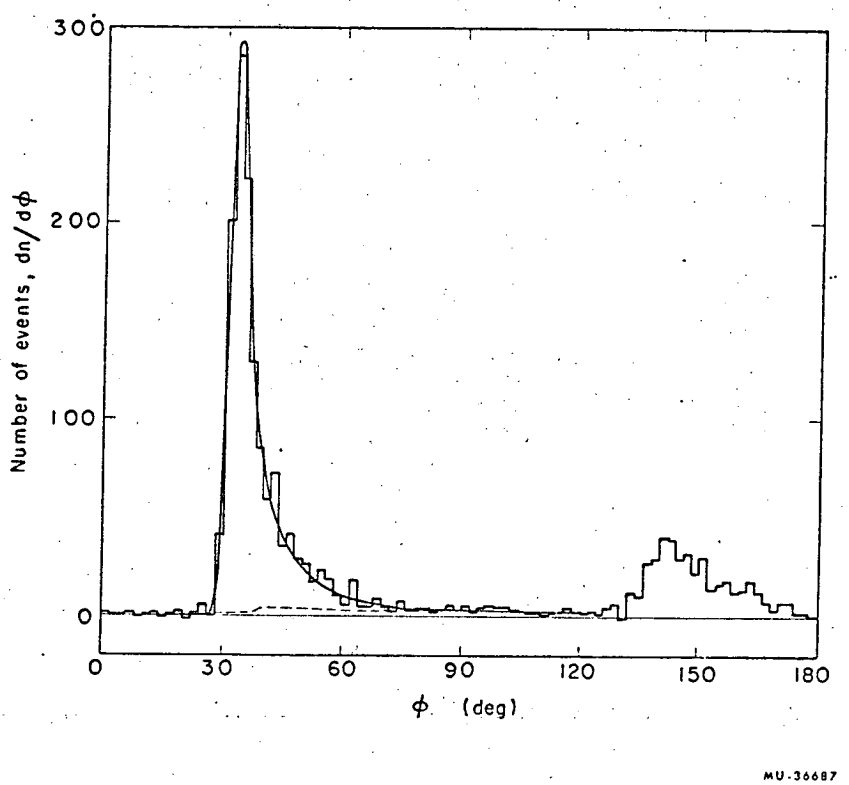
300
200
100
0
Number of events, dn/dφ
0
30
60
90
120
150
180
φ (deg)
MU-36687

Fig. 4

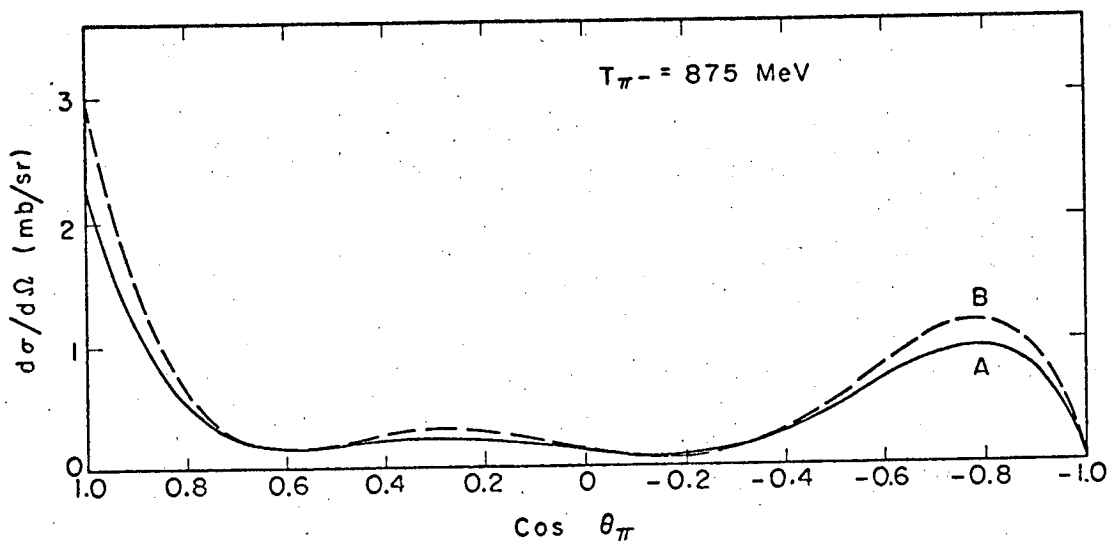

MU-36688

Fig. 5

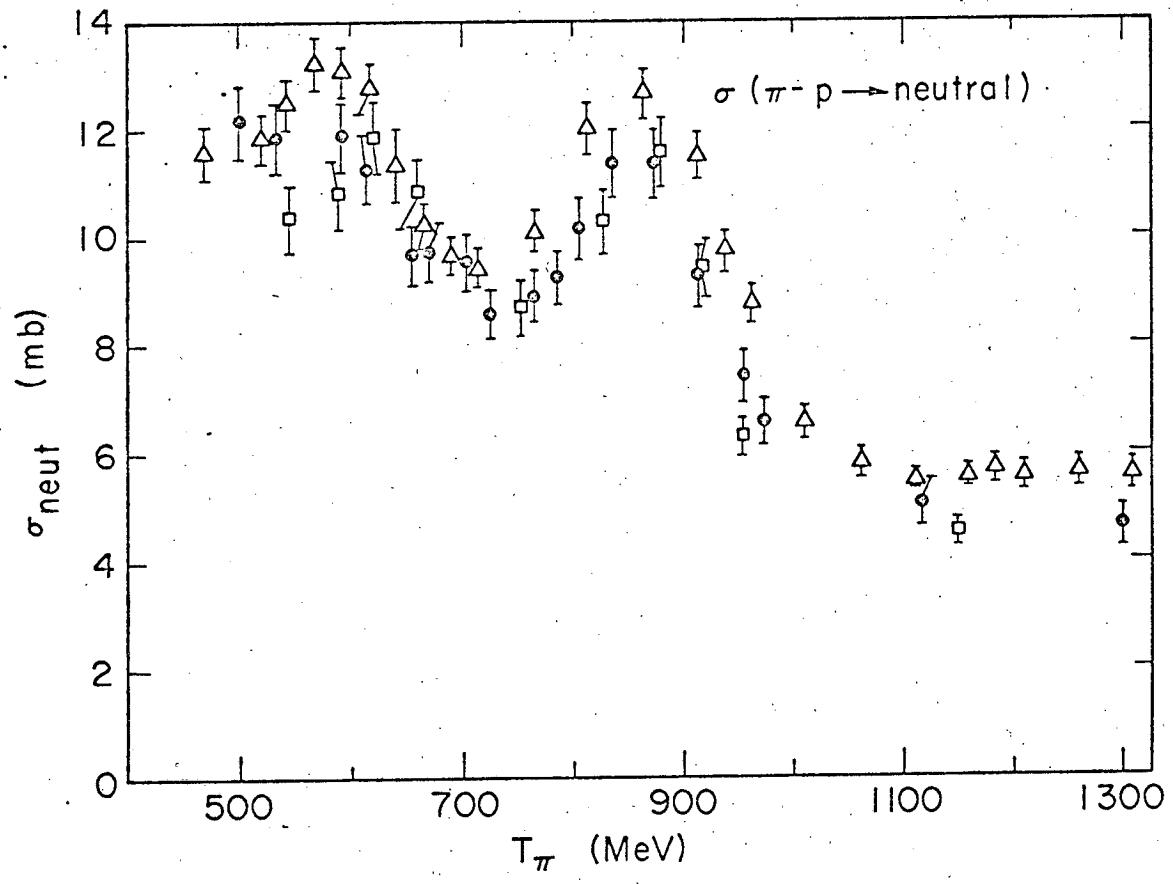

MUB-11384

Fig. 6

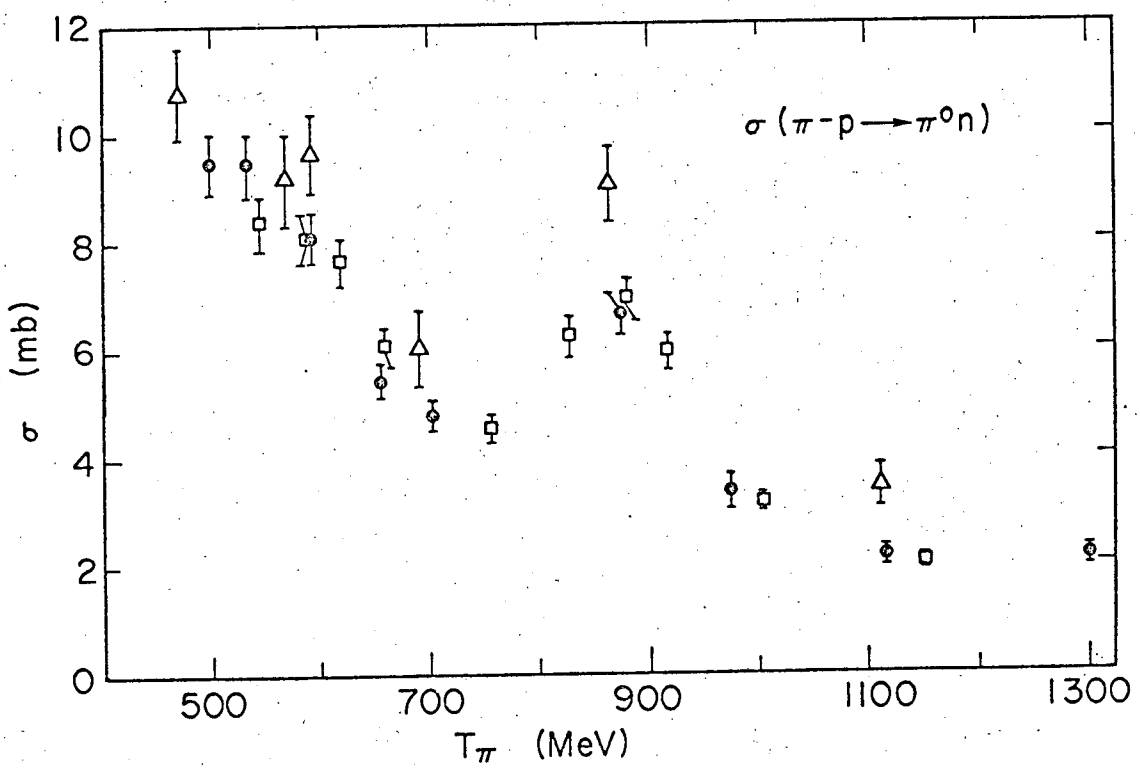

MUB-11385

Fig. 7

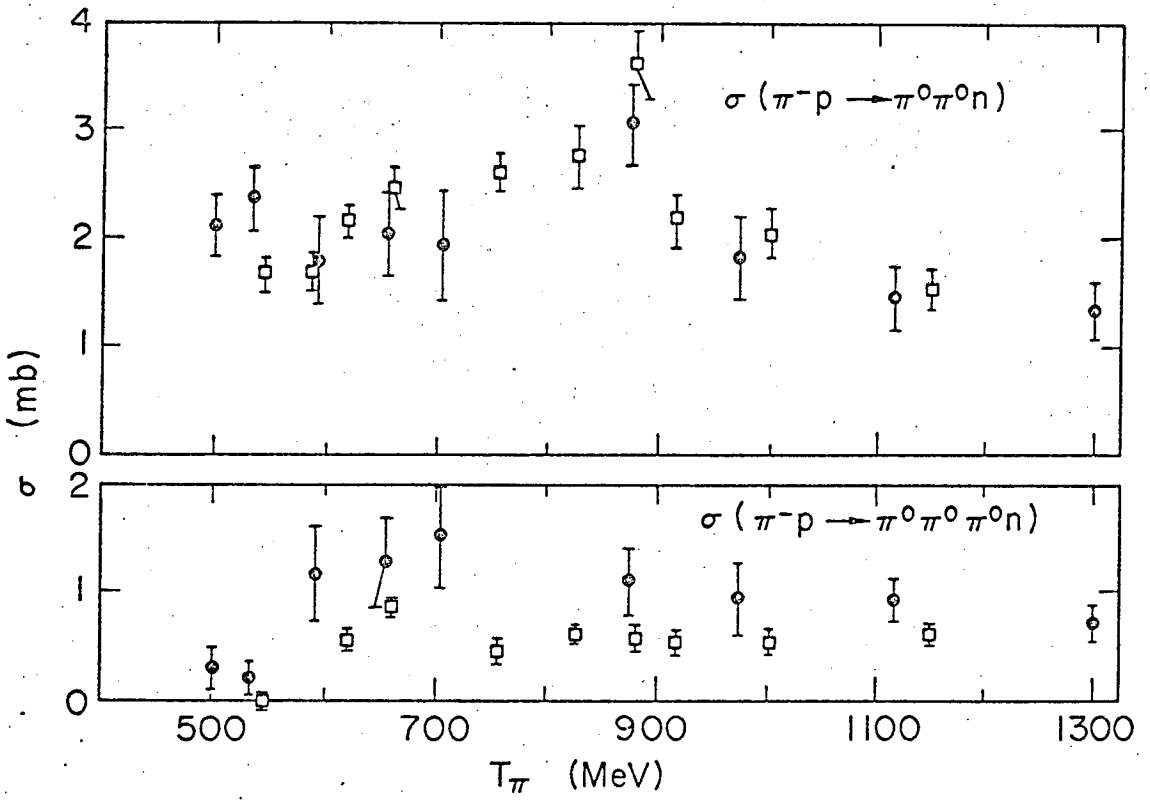

MUB-11386

Fig. 8

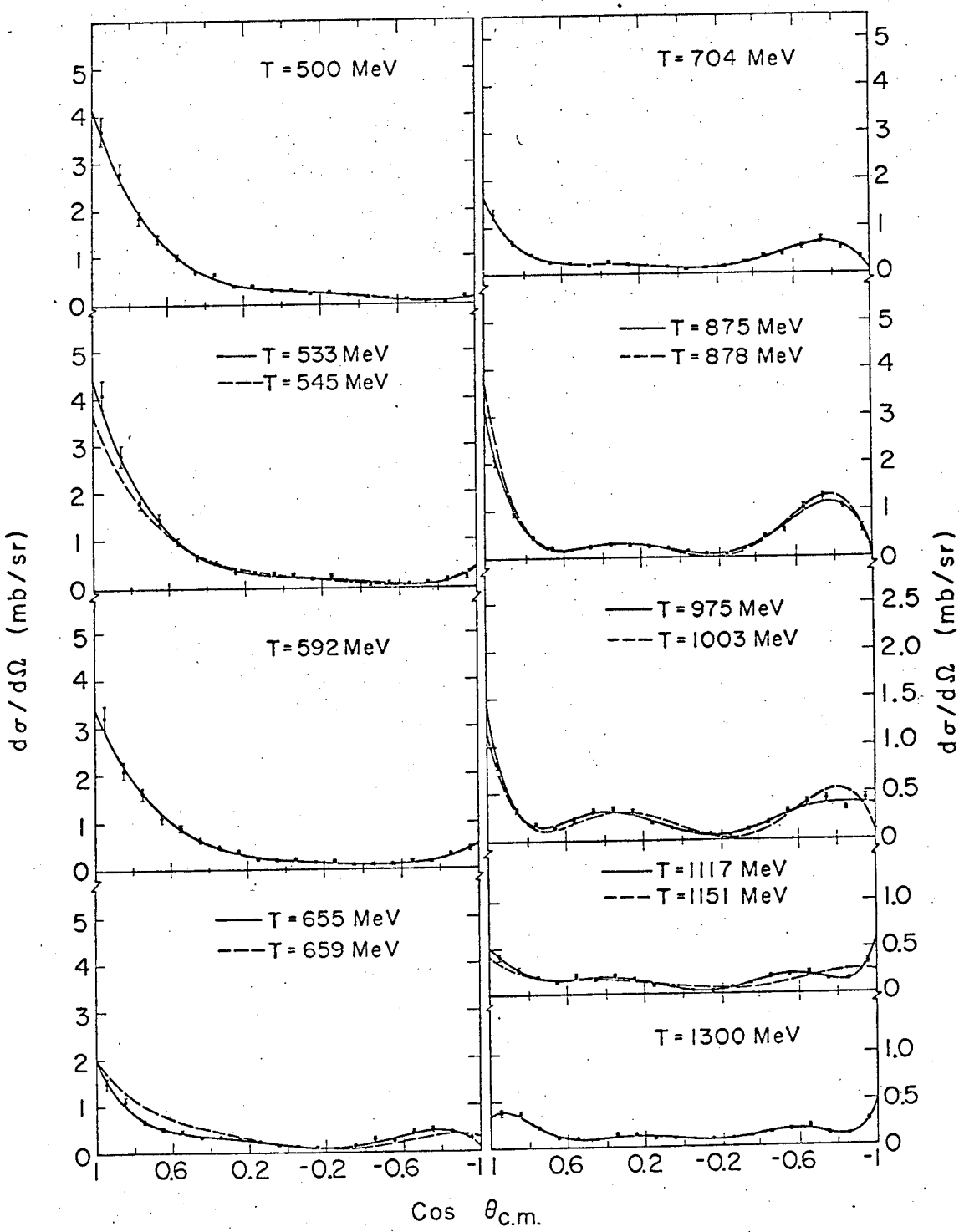
T = 500 MeV
T = 704 MeV
T = 533 MeV
T = 545 MeV
T = 875 MeV
T = 878 MeV
T = 592 MeV
T = 975 MeV
T = 1003 MeV
T = 655 MeV
T = 659 MeV
T = 1117 MeV
T = 1151 MeV
T = 1300 MeV
dσ/dΩ (mb/sr)
Cos θc.m.

Fig. 9

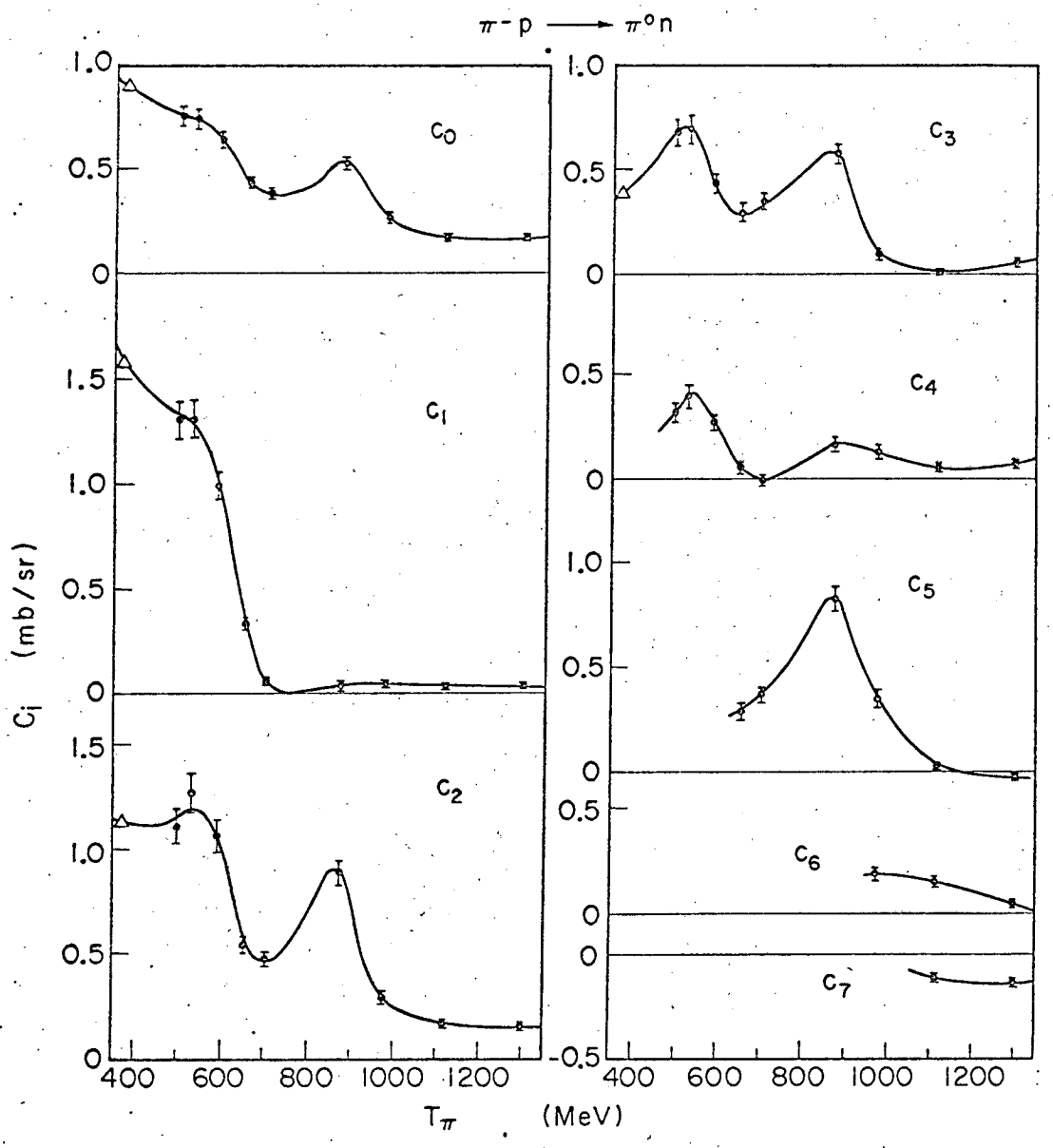

Fig. 10

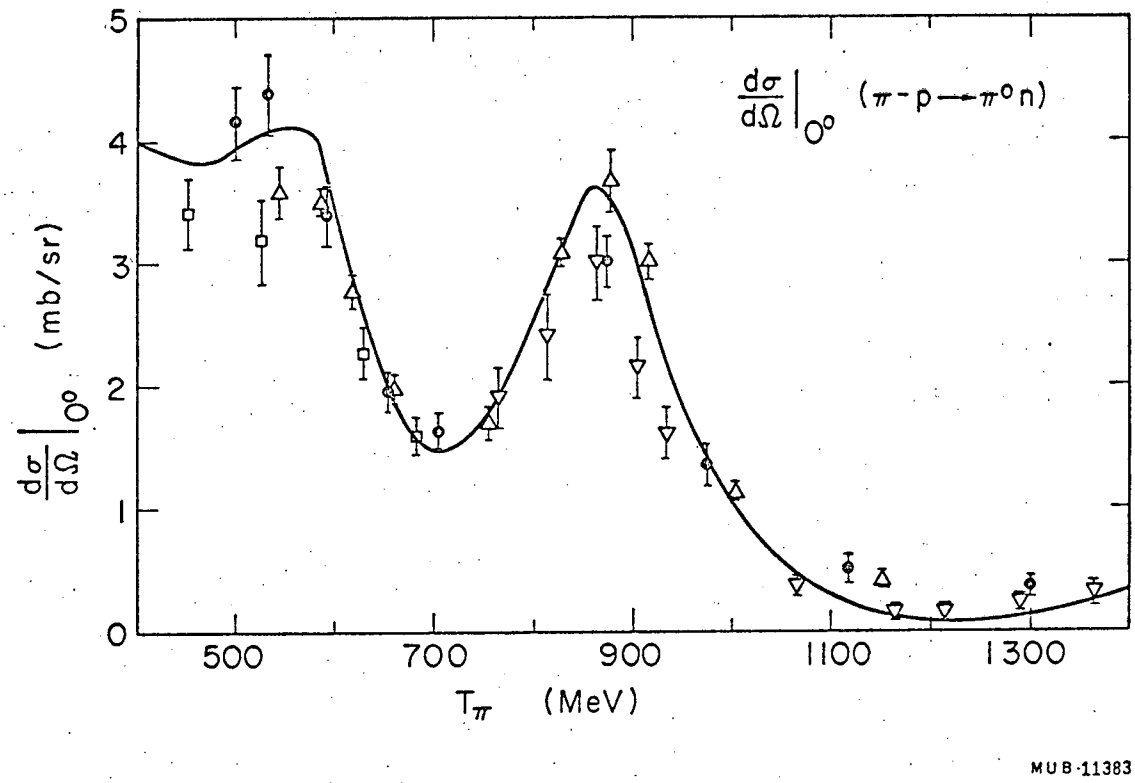
$\frac{d\sigma}{d\Omega}\Big|_{0^\circ}$ $(\pi^- p \rightarrow \pi^0 n)$
$\frac{d\sigma}{d\Omega}\Big|_{0^\circ}$ (mb/sr)
T_π (MeV)
0
1
2
3
4
5
500
700
900
1100
1300
MUB-11383

Fig. 11

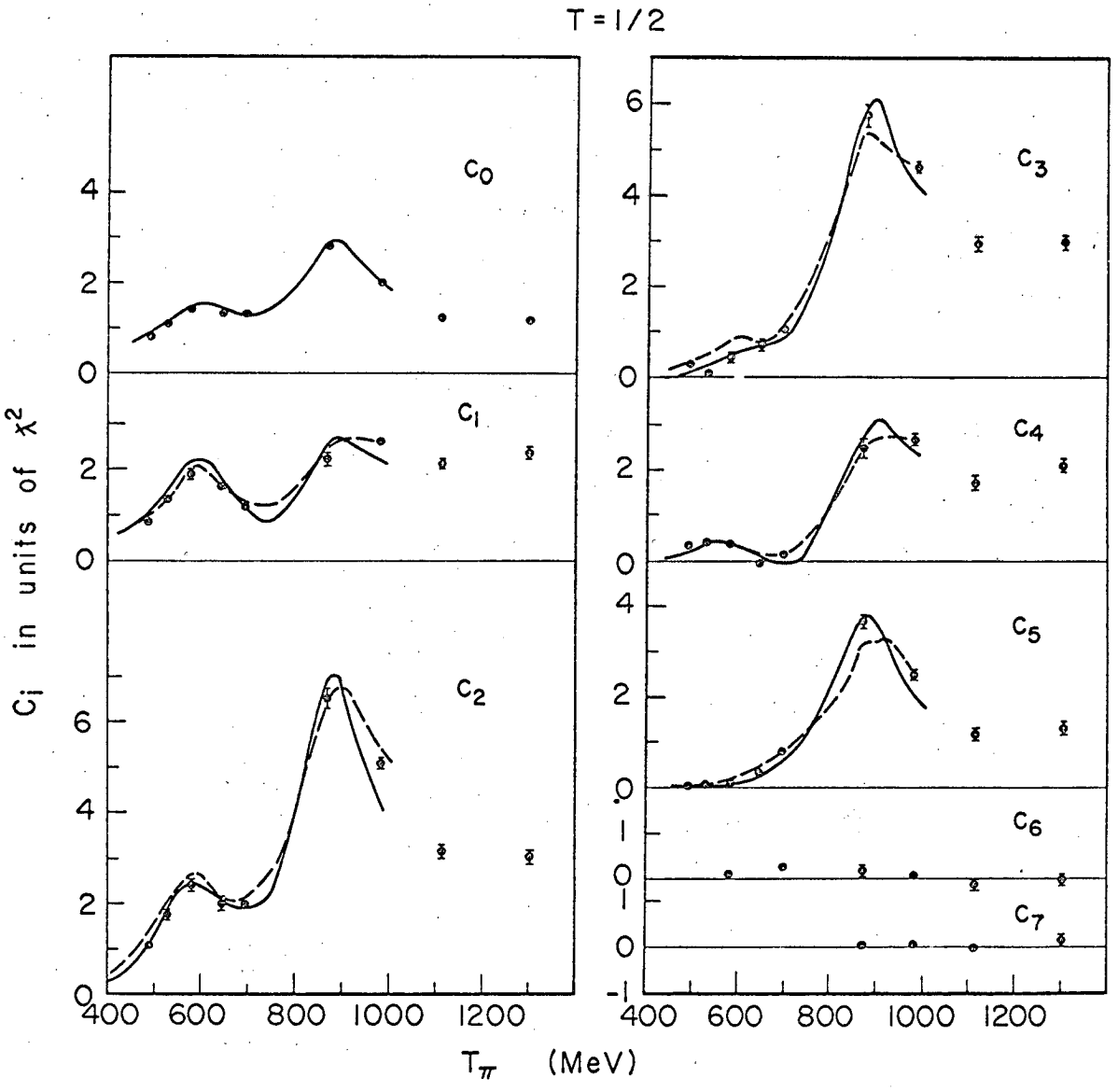
T = 1/2
C_0
C_1
C_2
C_3
C_4
C_5
C_6
C_7
C_i in units of λ^2
T_π (MeV)
400 600 800 1000 1200
MUB-11387

Fig. 12

This report was prepared as an account of Government sponsored work. Neither the United States, nor the Commission, nor any person acting on behalf of the Commission:

A. Makes any warranty or representation, expressed or implied, with respect to the accuracy, completeness, or usefulness of the information contained in this report, or that the use of any information, apparatus, method, or process disclosed in this report may not infringe privately owned rights; or

B. Assumes any liabilities with respect to the use of, or for damages resulting from the use of any information, apparatus, method, or process disclosed in this report.

As used in the above, "person acting on behalf of the Commission" includes any employee or contractor of the Commission, or employee of such contractor, to the extent that such employee or contractor of the Commission, or employee of such contractor prepares, disseminates, or provides access to, any information pursuant to his employment or contract with the Commission, or his employment with such contractor.